Heat Transfer Research 45(7), 677–700 (2014)

NUMERICAL SIMULATION OF MIXED CONVECTION IN A SiO_2/WATER NANOFLUID IN A TWO–SIDED LID-DRIVEN SQUARE ENCLOSURE WITH SINUSOIDAL BOUNDARY CONDITIONS ON THE WALL

Mohammad Hemmat Esfe, Seyed Sadegh Mirtalebi Esforjani, Mohammad Akbari, & Mohammad Hadi Hajmohammad*

Department of Mechanical Engineering, Najafabad Branch, Islamic Azad University, Isfahan, Iran

*Address all correspondence to Mohammad Hemmat Esfe
E-mail: M.hemmatesfe@gmail.com

To investigate mixed convection flows through a nanofluid in a square double lid-driven cavity with various inclination angles and sinusoidal heating on the left wall, a numerical method based on the finite volume approach is applied. In this work, a SiO_2–water nanofluid was used. The cavity is nonuniformly heated from the left, T_h, and cooled from the opposite wall. The top and the bottom moving walls were supposed to be insulated. The study was performed at the Richardson number from 0.1 to 10, Reynolds number from 1 to 100, and the solid volume fraction of nanoparticles φ altereing from 0 to 0.06. The effects of variations of Richardson and Reynolds number, angle of inclination, and solid volume fraction of nanoparticles on the hydrodynamic and thermal characteristics have been studied and discussed. As a result, it was found that the increases heat transfer rate with the solid volume fraction for a particular Re. The heat transfer rate also increases with the Richardson and Reynolds numbers for a particular volume fraction. The problem of mixed convection flows through a nanofluid in a square double lid-driven cavity with various inclination angles and sinusoidal temperature profiles on the left wall has not been reported so far. The effects of an increase in the shear force or buoyancy force, with another force kept constant, on heat transfer enhancement are studied.

KEY WORDS: *mixed convection, double lid-driven, numerical simulation, nanofluid*

1. INTRODUCTION

Mixed convection is a kind of convection including both natural and forced convection. Its significant role in many applications in industry and engineering has been specified: lake and reservoirs (Imberger and Hamblin, 1982), food processing, crystal growth (Moallemi and Jang, 1992), electronic cooling devices, drying technologies,

1064-2285/14/$35.00

NOMENCLATURE

c_p	specific heat, $J \cdot kg^{-1} \cdot K^{-1}$
g	gravitational acceleration, $m \cdot s^{-2}$
Gr	Grashof number
h	heat transfer coefficient, $W \cdot m^{-2} \cdot K^{-1}$
L	enclosure length, m
k	thermal conductivity, $W \cdot m^{-1} \cdot K^{-1}$
Nu	Nusselt number
p	pressure, $N \cdot m^{-2}$
P	dimensionless pressure
Pr	Prandtl number
q	heat flux, $W \cdot m^{-2}$
Re	Reynolds number
Ri	Richardson number
T	dimensional temperature, K
u, v	dimensional velocity components in x and y directions, $m \cdot s^{-1}$
U, V	dimensionless velocity components in X and Y directions
U_0	lid velocity
x, y	dimensional Cartesian coordinates, m
X, Y	dimensionless Cartesian coordinates

Greek symbols

α	thermal diffusivity, $m^2 \cdot s$
β	thermal expansion coefficient, K^{-1}
θ	dimensionless temperature
μ	dynamic viscosity, $kg \cdot m^{-1} \cdot s^{-1}$
ν	kinematic viscosity, $m^2 \cdot s^{-1}$
ρ	density, $kg \cdot m^{-3}$
φ	volume fraction of nanoparticles
γ	cavity inclination angle

Subscripts

c	cold
eff	effective
f	fluid
h	hot
nf	nanofluid
s	solid particles
w	wall

solar ponds (Cha and Jaluria, 1984), solar collectors (Ideriah, 1980), and float glass production (Pilkington, 1969) are among its current applications. The complexity of this type of heat transfer is the coupling between the buoyancy force created by a temperature difference on the boundary of a convection zone and shear force created by the wall movement.

Different types of nondimensional parameters used to delineate the flows are: the Grashof number (Gr), Reynolds number (Re), and the Prandtl number (Pr). Among other important nondimensional parameters the Richardson number can be mentioned. The Richardson number is the measure of the relative importance of the buoyancy-driven natural convection compared to forced convection. Based on the values of the Richardson number, the problem of the mixed shear and buoyancy-driven convec-

tion can be divided into three flow regimes as follows: pure natural convection for Ri >> 1, pure forced convection for Ri << 1, and mixed convection for 0.1 < Ri < 10 (Aydin, 1999).

Many researches have been conducted on mixed-convection heat transfer in different configurations and mixtures with thermal boundary conditions that idealize problems for many practical engineering and industrial applications. Due to the practical significance of mixed-convection heat transfer in a cavity with different configurations, it has attracted much attention during the last few decades (Basak et al., 2009; Mahmoodi, 2011; Sebdani et al., 2012; Rahman et al., 2008).

In most of them, conventional fluids (such as water, ethylene glycol, etc.) were used. But the serious problem of these common heat transfer fluids is their low thermal conductivity.

To overcome this problem, an innovative technique, i.e., the use of nanoscale particles in the base fluid, has been adopted. Choi (1995) called these fluids nanofluids.

The problem of heat transfer by using a nanofluid has been the topic of intensive analytical, numerical, and experimental investigations in the recent years.

As an example, Masuda et al. (1993) found that if only 0.3% volume fraction of nanoparticles is dispersed in a liquid, 20% improvement of the effective thermal conductivity of ethylene glycol occurs. In another research Lee et al. (1999) showed that an increase in the solid volume fraction results in the increase of the thermal conductivity of nanofluids. He also found that the size of a nanoparticle plays an important role in improvement of the thermal conductivity of nanofluids. In another study, a numerical investigation of heat transfer improvement by using nanofluids in forced convection flows was done by Maiga et al. (2005). The results revealed that a noticeable augmentation of the heat transfer coefficient occurs that definitely increases with increase of particles in the base fluid.

As mentioned above, an increase in the number of nanoparticles in the base fluid increases the thermal conductivity of the nanofluid. However, the shape, size, and thermal properties of solid particles in nanofluids exert an important effect on the thermal conductivity (Eastman et al., 2001), but the role of the extensive contact surface of nanoparticles in the enhancement of heat transfer is more significant than the role of larger particles (Xuan and Li, 2000).

Some works were done on the cavity filled with a nanofluid. For instance, Hwang et al. (2007) presented numerical simulation of natural convection in a rectangular cavity filled with an Al_2O_3 nanofluid heated from bellow. They used different models to measure the effective thermal conductivity.

Their results show that as the volume fraction of the nanofluid increases, the size of nanoparticles decreases, or the average temperature of nanofluids increases and that Al_2O_3 nanofluids are more stable than the base fluid in a rectangular cavity.

Moreover, heat transfer enhancement in a cavity was investigated by Wen and Ding (2005). Their rectangular cavity was filled with a water–TiO_2 nanofluid heated from

below. They found that for the Rayleigh number less than 10^6, at a specific Rayleigh number, the natural convection heat transfer rate decreases as the particle concentration increases.

Due to the importance of lid-driven cavity, many researchers investigated it in various configurations. For example, Mohammad and Viskanta (1995) performed a numerical survey of a two- and three-dimensional laminar mixed-convection flow in a shallow driven enclosure heated from below where water was utilized.

In addition, few researches investigated mixed convection with a lid-driven cavity. First, Tiwari and Das (2007) conducted a numerical study of heat transfer enhancement in a lid-driven square cavity filled with a Cu–water nanofluid, and with insulated top and bottom walls. With regard to the movement of the walls in different directions, they studied their effects on the heat transfer and fluid flow in the cavity. Their results show that with increase in the volume fraction of nanoparticles, the average Nusselt number also increases for the Richardson number equal to unity. A numerical investigation of laminar mixed-convective heat transfer in rectangular lid-driven cavities of aspect ratio 10 was performed by Sharif (2007). In his work, the moving top wall is kept at a higher temperature than the lower fixed wall. The impacts of the inclination angle were investigated for angels ranging from 0 to 30. He found that on the top moving wall, the local Nusselt number decreased substantially as it moved towards the right side.

In another work, Muthtamilselvan et al. (2010) carried out a numerical investigation of the mixed-convection flow in a lid-driven rectangular enclosure subjected to a copper–water nanofluid. They surveyed effects of the aspect ratio and nanoparticle concentration on the fluid flow and heat transfer in the cavity.

A numerical survey of mixed-convection heat transfer in a lid-driven cavity filled with an Al_2O_3 nanofluid was made by Zarei et al. (2013). They reported that the heat transfer rate increased inside the cavity with increase in the volume fraction of nanoparticles.

The numerical study of mixed convection in a square lid-driven cavity partially heated from below and filled with a water-base nanofluid was performed by Mansuor et al. (2010). Their results show that the average Nusselt number increases on increase in the volume fraction of nanoparticles. Numerical investigation of mixed convection in a lid-driven triangular enclosure filled with a water–Al_2O_3 nanofluid and having an insulated horizontal wall, hot inclined wall, and a moving cold vertical wall was made by Ghasemi and Aminossadati (2010). They found that addition of Al_2O_3 nanoparticles improves the rate of heat transfer for each direction of the sliding wall motion and for all values of Richardson number. Moreover, some studies were focused on cavities with nonuniformly temperature distribution on their walls.

Natural convection in a rectangular, 2D cavity under adiabatic conditions on the bottom and side walls and sinusoidal temperature profile on the upper wall was studied numerically by Sarris et al. (2002). A numerical study was performed by Basak

et al. (2006) to investigate the effects of thermal boundary conditions on a steady laminar natural-convection flow in an air-filled square enclosure with a uniformly heated and adiabatic top wall and constant temperature of the cold vertical walls, as well as nonuniformly heated bottom wall. Sathiyamoorthy et al. (2007) numerically studied steady natural-convection flows in a square enclosure with the bottom wall uniformly heated and vertical wall(s) heated linearly. Mixed convection in the presence of a magnetic field in a lid-driven cavity with sinusoidal boundary conditions on both sidewalls was investigated numerically by Sivasankaran et al. (2011). Despite the mentioned works, only few works were done on natural or mixed convection of nanofluids in cavities with a nonuniformly heated wall. The steady state analysis of natural convection problem in an inclined cavity filled with TiO_2–water and Al_2O_3–water was investigated numerically by Oztop et al. (2011) and also on using heating and cooling with sinusoidal temperature profiles on one side.

Within the knowledge of the authors, the problem of mixed-convection flows through a nanofluid in a square double lid-driven cavity with various inclination angles and with sinusoidal temperature profiles on the left wall has not been reported so far. Effects of increased shear force or buoyancy force, with the other force kept constant, on heat transfer enhancement were studied. Our results include streamlines, temperature field, and average Nusselt number which can be different completely from horizontal configurations and a uniform temperature profile.

2. PROBLEM DEFINITION AND MATHEMATICAL FORMULATION

Figure 1 shows a two-dimensional square double lid-driven cavity considered in the present study. The cavity is filled with a suspension of SiO_2 nanoparticles in water.

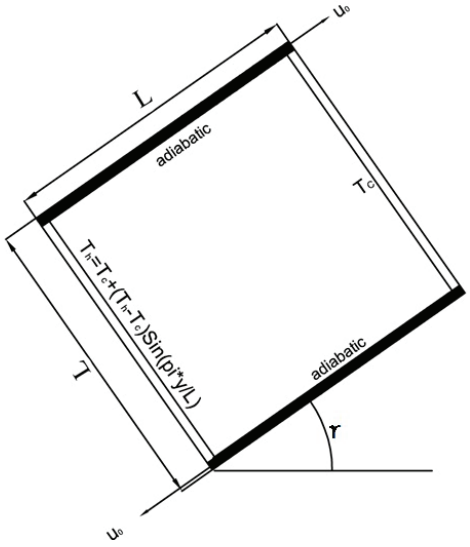

FIG. 1: Schematic diagram of the double lid-driven cavity considered in the present study

TABLE 1: Thermophysical properties of different phases

Solid (Al_2O_3)	Fluid phase (water)	Physical properties
765	4179	c_p (J/kg·K)
3970	997.1	ρ (kg/m^3)
36	0.6	K (W·m^{-1}·K^{-1})
118.536	1.47	$\alpha \times 10^{-5}$
0.63	21	$\beta \times 10^{-5}$ (1/K)
……..	9.9	$\mu \times 10^{-4}$(kg/m·s)
80	.....	d_p (nm)

The shape and size of the solid particles are assumed to be uniform. The diameter of the nanoparticle is assumed to be 80 nm.

The cavity is cooled from the right wall (T_c), while a sinusoidal temperature profile exists on its left wall. The top moving and bottom moving walls were supposed to be insulated.

Except for the density, the properties of the nanoparticles and fluid are taken to be constant. Table 1 presents the thermophysical properties of water and copper at the reference temperature. It is further assumed that the Boussinesq approximation is valid for the buoyancy force. The governing equations for a steady, two-dimensional laminar and incompressible mixed convection flow are expressed as below.

The viscosity and thermal conductivity of the nanofluid vary with the volume fraction of the nanoparticles. The governing equations are

$$\frac{\partial u}{\partial x} + \frac{\partial v}{\partial y} = 0\,, \tag{1}$$

$$u\,\frac{\partial u}{\partial x} + v\,\frac{\partial u}{\partial y} = -\,\frac{1}{\rho_{nf}}\,\frac{\partial p}{\partial x} + \upsilon_{nf}\nabla^2 u + + \frac{(\rho\beta)_{nf}}{\rho_{nf}}\,g\Delta T\,\sin\,(\gamma)\,, \tag{2}$$

$$u\,\frac{\partial v}{\partial x} + v\,\frac{\partial v}{\partial y} = -\,\frac{1}{\rho_{nf}}\,\frac{\partial p}{\partial y} + \upsilon_{nf}\nabla^2 v + \frac{(\rho\beta)_{nf}}{\rho_{nf}}\,g\Delta T\,\cos\,(\gamma)\ . \tag{3}$$

Energy:

$$u\,\frac{\partial T}{\partial x} + v\,\frac{\partial T}{\partial y} = \alpha_{nf}\nabla^2 T\ . \tag{4}$$

The dimensionless form of the governing equation can be obtained by applying the following dimensionless parameters:

$$X = \frac{x}{L}, \quad Y = \frac{y}{L}, \quad V = \frac{v}{U_0}, \quad U = \frac{u}{U_0},$$

$$\Delta T = \frac{q''L}{k_f}, \quad \theta = \frac{T - T_c}{\Delta T}, \ \mathrm{Pr} = \frac{\upsilon_f}{\alpha_f}, \tag{5}$$

$$P = \frac{p}{\rho_{nf} U_0^2} \quad \mathrm{Ra} = \frac{g\beta_f q'' L^4}{k_f \upsilon_f \alpha_f}.$$

Equations (6) to (9) are the dimensionless form of Eqs. (1) to (4):

$$\frac{\partial U}{\partial X} + \frac{\partial V}{\partial Y} = 0, \tag{6}$$

$$U\frac{\partial U}{\partial X} + V\frac{\partial U}{\partial Y} = -\frac{\partial P}{\partial X} + \frac{\upsilon_{nf}}{\upsilon_f}\frac{1}{\mathrm{Re}}\nabla^2 U + \frac{\mathrm{Ri}}{\mathrm{Pr}}\frac{\beta_{nf}}{\beta_f}\Delta\theta \sin(\gamma), \tag{7}$$

$$U\frac{\partial V}{\partial X} + V\frac{\partial V}{\partial Y} = -\frac{\partial P}{\partial Y} + \frac{\upsilon_{nf}}{\upsilon_f}\frac{1}{\mathrm{Re}}\nabla^2 V + \frac{\mathrm{Ri}}{\mathrm{Pr}}\frac{\beta_{nf}}{\beta_f}\Delta\theta \cos(\gamma), \tag{8}$$

$$U\frac{\partial \theta}{\partial X} + V\frac{\partial \theta}{\partial Y} = \frac{\alpha_{nf}}{\alpha_f}\nabla^2\theta. \tag{9}$$

The thermal diffusivity and effective density can be obtained by applying the following equations:

$$\alpha_{nf} = \frac{k_{nf}}{(\rho c_p)_{nf}}, \tag{10}$$

$$\rho_{nf} = \varphi\rho_s + (1 - \varphi)\rho_f. \tag{11}$$

The heat capacitance and thermal expansion coefficient of the nanofluid are defined as

$$(\rho c_p)_{nf} = \varphi(\rho c_p)_s + (1 - \varphi)(\rho c_p)_f, \tag{12}$$

$$(\rho\beta)_{nf} = \varphi(\rho\beta)_s + (1 - \varphi)(\rho\beta)_f. \tag{13}$$

The effective dynamic viscosity of the SiO_2–water nanofluid is calculated according to the Brinkman model as follows:

$$\mu_{nf} = \frac{\mu_f}{(1 - \varphi)^{2.5}}. \tag{14}$$

Several relations can be used to express the effective thermal conductivity of the nanofluid. In this study, it is approximated by the Patel model:

$$\frac{k_{nf}}{k_f} = 1 + \frac{k_s A_s}{k_f A_f} + c k_s \ \mathrm{Pe}\ \frac{A_p}{k_f A_f} \ , \tag{15}$$

where c is constant and must be determined experimentally, A_s/A_f and Pe are defined as

$$\frac{A_s}{A_f} = \frac{d_s}{d_f}\frac{\varphi}{1-\varphi} \ , \ \mathrm{Pe} = \frac{u_s d_s}{\alpha_f} \ ,$$

where d_s is the diameter of the solid particles which is assumed in this study to be equal to 80 nm, d_f is the molecular size of liquid taken to be 2 Å for water. Also, u_s is the Brownian motion velocity of nanoparticle which is defined as

$$u_s = \frac{2k_b T}{\pi \mu_f d_s^2} \ ,$$

where k_b is the Boltzmann constant.

In order to investigate the heat transfer enhancement, the local Nusselt number is defined by Eq. (16) and the average Nusselt number over cold surfaces is expressed by Eq. (17).

$$\mathrm{Nu} = \frac{hL}{k_f} \ , \tag{16}$$

$$\mathrm{Nu}_m = \frac{1}{L}\int_0^L \mathrm{Nu}\ dY \ . \tag{17}$$

The boundary conditions are

left wall:

$$\begin{cases} U = V = 0 \\ \theta = \sin(\pi Y) \end{cases} .$$

right wall:

$$\begin{cases} U = V = 0 \\ \theta = 0 \end{cases} .$$

bottom wall:

$$\begin{cases} U = -1, V = 0 \\ \dfrac{\partial \theta}{\partial Y} = 0 \end{cases} .$$

top wall:

$$\begin{cases} U = 1, V = 0 \\ \dfrac{\partial \theta}{\partial Y} = 0 \end{cases} . \tag{18}$$

3. NUMERICAL METHOD

The continuity, momentum, and energy balance equations have been solved by a control-volume numerical code. The SIMPLE algorithm has been used for the pressure–velocity coupling. The convection terms are approximated by a combination of the hybrid-scheme which is conducive to a stable solution. Furthermore, a second-order central differencing scheme is used for the diffusion terms. The algebraic system resulting from numerical discretization was solved utilizing the Tridiagonal Matrix Algorithm (TDMA) applied to a line going through all volumes in the computational domain. The solution procedure is iterated until the following convergence criterion is satisfied:

$$rror = \frac{\sum_{j=1}^{j=M}\sum_{i=1}^{i=N}\left|\lambda^{n+1}-\lambda^{n}\right|}{\sum_{j=1}^{j=M}\sum_{i=1}^{i=N}\left|\lambda^{n+1}\right|} < 10^{-7}. \tag{19}$$

Here, M and N correspond to the number of grid points in the x and y directions, respectively, n is the number of iteration, and λ denotes any scalar transport quantity. To study the effect of the grid size on the results, several cases were investigated by changing the number of grid points in a uniform mesh. The results of this study are listed in Table 2 for various cases. Grid independence was achieved with a grid of size 121 × 121.

In order to assess the accuracy of the results, a complete analysis of studies (Tiwari and Das, 2007; de Vahl Davis, 1983; Markatos and Pericleous, 1984; Hadjisophocleous et al., 1998; Fusegi et al., 1991; Ha and Jung, 2000) has been made. Computations were carried out for 15 different Re and Gr combinations. Comparisons between the average Nu numbers at the hot lid are shown in Table 3 where an excellent agreement is confirmed, thus ensuring their validation.

TABLE 2: Mesh validating

Mesh size	Nu	Nu
	φ = 0.02, Re = 1, Ri = 1	**φ = 0.06, Re = 100, Ri = 10**
41 × 41	0.709	5.796
61 × 61	0.713	5.823
81 × 81	0.715	5.816
101 × 101	0.716	5.801
111 × 111	0.716	5.771
121 × 121	0.717	5.771
131 × 131	0.717	5.770

TABLE 3: Comparison of solutions for natural convection in an enclosed cavity

	Present study	**de Vahl Davis (1983)**	**Markatos and Pericleous (1984)**	**Hadjisophocleous et al. (1998)**	**Tiwari and Das (2007)**	**Fusegi et al. (1991)**	**Ha and Jung (2000)**
$Ra = 10^3$							
Nu	1.1366	1.118	1.108	1.141	1.0871	1.085	1.072
Nu_{max}	1.5738	1.505	1.496	1.540	1.508		
Nu_{min}	0.6468	0.692	0.72	0.727	0.6901		
$Ra = 10^4$							
Nu	2.3256	2.243	2.201	2.29	2.195	2.1	2.070
Nu_{max}	3.5456	3.528	3.482	3.84	3.5585		
Nu_{min}	0.7172	0.586	0.643	0.670	0.5809		
$Ra = 10^5$							
Nu	4.4928	4.519	4.430	4.964	4.450	4.361	4.464
Nu_{max}	7.3037	7.117	7.626	8.93	7.9371		
Nu_{min}	0.9906	0.729	0.824	1.01	0.7173		
$Ra=10^6$							
Nu	8.6388	8.799	8.754	10.39	8.803		
Nu_{max}	14.2521	17.925	17.872	21.41	19.2675		
Nu_{min}	1.6247	0.989	1.232	1.58	0.9420		

4. RESULTS AND DISCUSSION

In this paper, we investigated natural- and forced-convection heat transfer in a square enclosure with the top wall moving to the right and the bottom wall to the left. The top and bottom walls of the cavity mentioned were insulated while the left wall was exposed to a sinusoidal temperature and the right wall was maintained at a constant low temperature T_c. Flow and temperature fields, average Nusselt number for silicon oxide nanoparticles at Re varying from 1 to 300, Ri from 0.1 to 1, φ from 0 to 0.06, and γ from 0^o to 150^o are obtained and discussed. These results include an isotherm plot, streamlines, and values of the average Nusselt number. Plots of the streamlines and the isotherm for Ri = 1, and different Re and γ numbers for the nanofluid (φ = 0.06) and base fluid are shown in Figs. 2 and 3.

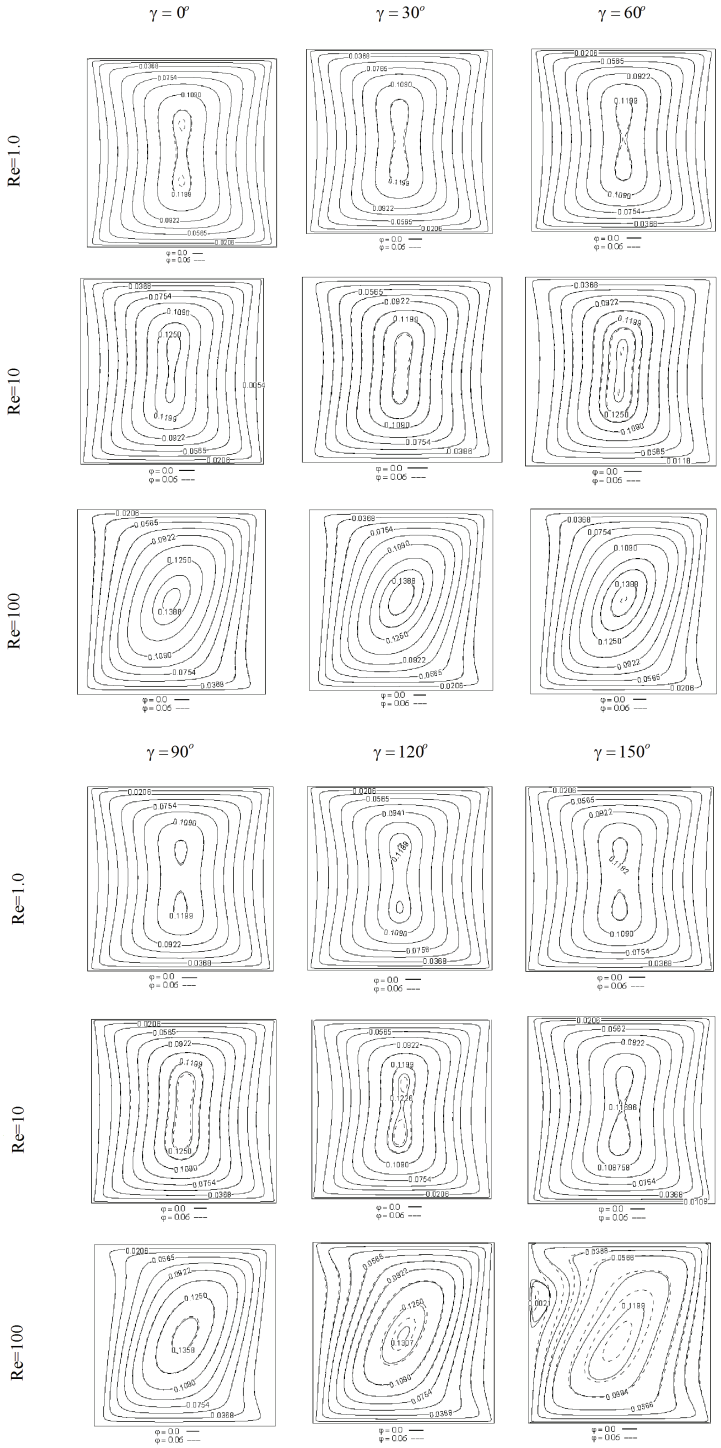

FIG 2: Streamlines for various Re and γ at Ri = 1

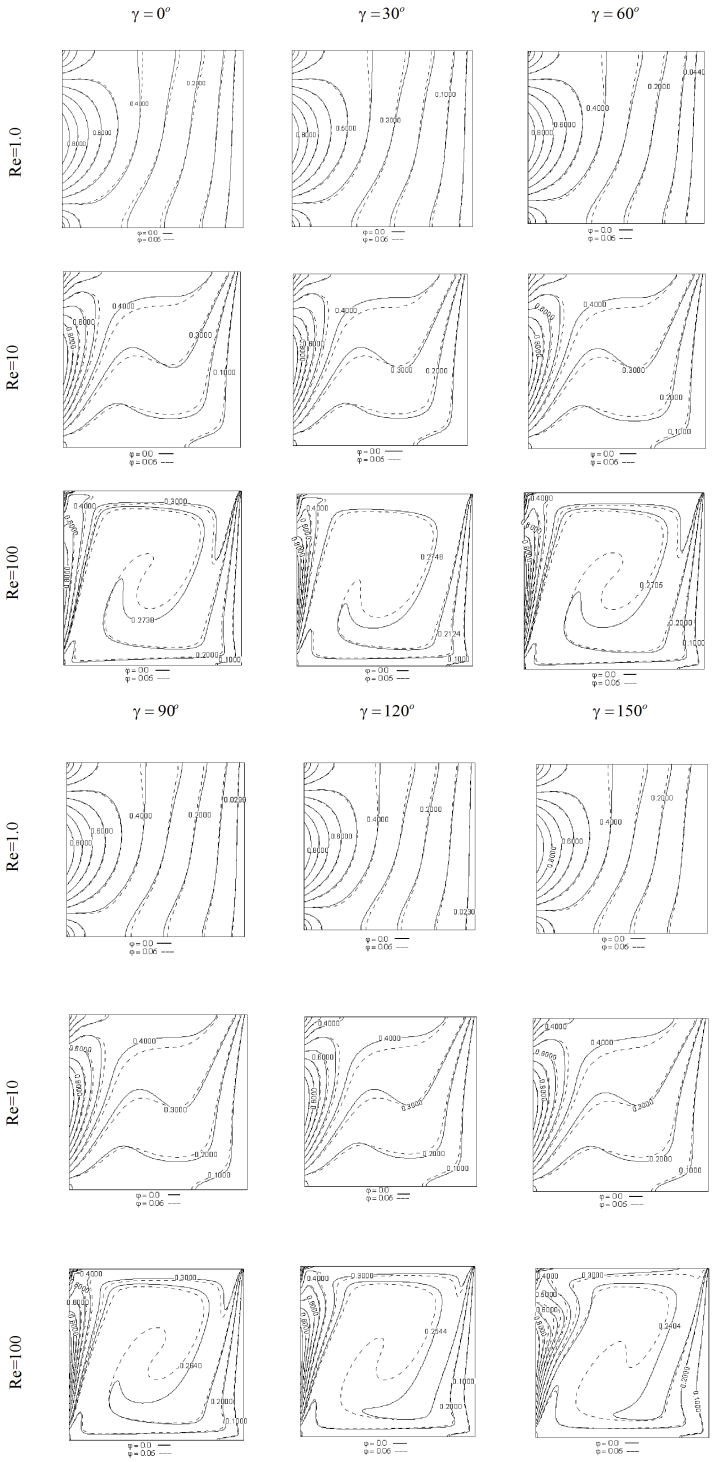

FIG 3: Isotherm for various Re and γ at Ri = 1

As can be seen from these figures, an increase of the Re number at a specified γ increases the intensity of the streamlines. Therefore, the mass flow rate between two specific points increases, and this phenomenon leads to an increase in the rate of heat transfer and in the average Nusselt number. Increasing φ does not have a considerable effect on the streamlines. However, in some figures related to Re = 100, the streamlines are located close to the wall. When $\gamma = 150^{o}$, the fluid is heated and consequently it flows upward, while the movement of the walls causes the nanofluid to move downward.

Therefore in the lower area of the heated wall a small vortex is formed at this slope. On increase in φ, the streamlines tend to get closer to the walls. So the value of the rate of mass flow near the heat source increases thus increasing the rate of heat transfer. For Re = 100 and $\gamma = 150^{o}$, an increase in φ leads to a decrease in the size of the vortex formed near the heat source surface.

At $\gamma = 0^{o}$ and at a lower Reynolds number, due to the slow movement of the upper and lower walls, the streamlines are located closer to these walls, than to the left and right walls, thus forming a vertically stretched vortex in the center of the cavity. In the upper and lower areas of this vortex, two small rotational flows are formed. On increase in the Re number up to 10 and then to 100, the velocity of the horizontal walls increases which causes a horizontal stretch in the fluid. Therefore, the height of the central vortex decreases.

Figure 3 shows the temperature field for Ri = 1. The temperature distribution near the heated wall is due to the sinusoidal form of temperature. As expected, the temperature is maximum at the center and is minimum at the corners of the upper and lower areas of the left wall. The fluid near the heated wall is expanded and moves upward due to the presence of the buoyancy force. As is mentioned before, the upper portions of the left wall have a lower temperature. Therefore, the heated fluid eventually encounters the portion of the wall that has lower temperature than the fluid. This phenomenon causes the heat transfer from the warm fluid to the cooler wall. Thus the total heat transfer decreases and its value would be negative with respect to the direction of the heat transfer in this local.

On increase in the Re number at specified Ri and γ, the intensity of the streamlines near the walls and the temperature gradient of the surface increase. Therefore, the average Nusselt number is expected to increase. After that the flow comes in contact with the sinusoidally heated wall that moves upward for a short time in the lower left portion of the cavity. When the warm fluid comes in contact with the upper section of the left wall which is cooler than the fluid, it loses some energy and the buoyancy force increases.

At a low Re number, the increase in the angle does not cause a significant change in the temperature fields. This is due to the fact that heat is transferred by both forced and natural convection. The low forced-convection heat transfer is due to the low Re number. It can be understood from the figures that the main cause of the natural heat convection is conduction which does not vary considerably with the angle.

On increase in the Reynolds number, the forced convection heat transfer rate also increases. At $\gamma = 0$, the buoyancy force acts in the same direction as the force caused by the movement of the top and the lower bottom walls. In this case, fluid loses some heat due to the contact with the cooler parts of the left wall. On increase in γ from 0^o to 90^o, the buoyancy force causes an upward motion in the fluid, while the moving walls cause a horizontal movement of the fluid. In this case, the fluid leaves the areas of the heated wall which is cooler than the fluid, thus the temperature of fluid located far from the heated wall increases. A further increase in γ up to 150^o makes this phenomenon more obvious.

At Re = 1, on increase in φ from 0 to 0.06, the isotherm lines spread in the lower section of the cavity. In the upper section of the cavity, the temperature lines get closer to the heated wall. Since the lower area of the heat source is cooler than the upper area, for both cases the rate of heat transfer increases with the volume fraction of nanoparticles. This trend is also valid for all angles. On increase in the Re number, the isotherm lines are distributed farther from the heated wall. So the points located farther from the heated wall have a higher temperature as compared to the lower volume fraction of nanoparticles, thus the amount of energy entering the cavity increases.

At Re = 1, the isotherm lines are almost parallel in the right section of the cavity. In this area, conduction heat transfer occurrs in the vertical layers of the fluid. Due to the insulation of the bottom and top walls, on increase of Re up to 100, the conduction heat transfer occurs between the horizontal layers in the central area of the cavity. On a further increase in the Re number, the conduction heat transfer occurs in the smaller area of the cavity, near the top and the bottom walls.

Figure 4 shows the streamlines at $\gamma = 30^o$ for different values of Ri and Re numbers. At this value of γ, on increase in the Re number, a stronger flow field is formed inside the cavity. On increase in the Ri number from 0.1 to 10, the forced convection heat transfer becomes stronger. Since the buoyancy force caused by the temperature gradient at $\gamma = 30^o$ is somewhat concurrent with the force caused by the movement of the walls, the fluid flow becomes stronger and the streamlines approach the surface, so that the area of the vortex in the center of the cavity increases.

Figure 5 demonstrates the temperature field at $\gamma = 30^o$. On increase in Re, the streamlines get closer to the sidewalls, thus the temperature gradient increases at a certain distance and the heat transfer rate also increases. On increase in Ri, the isotherm lines become concentrated on the heated wall. Also on increase in φ from 0 to 0.06, the rate of heat transfer increases for all the cases.

Figure 6 shows the variation of the average Nusselt number with Ri and φ for different values of Re at $\gamma = 0^o$. For Re = 1, the variations of Ri do not cause a considerable effect on the average Nusselt number. But at high Re numbers, a change in Ri causes a significant change in the Nusselt number. The Nusselt numbers for other γ values are also listed in Table 4.

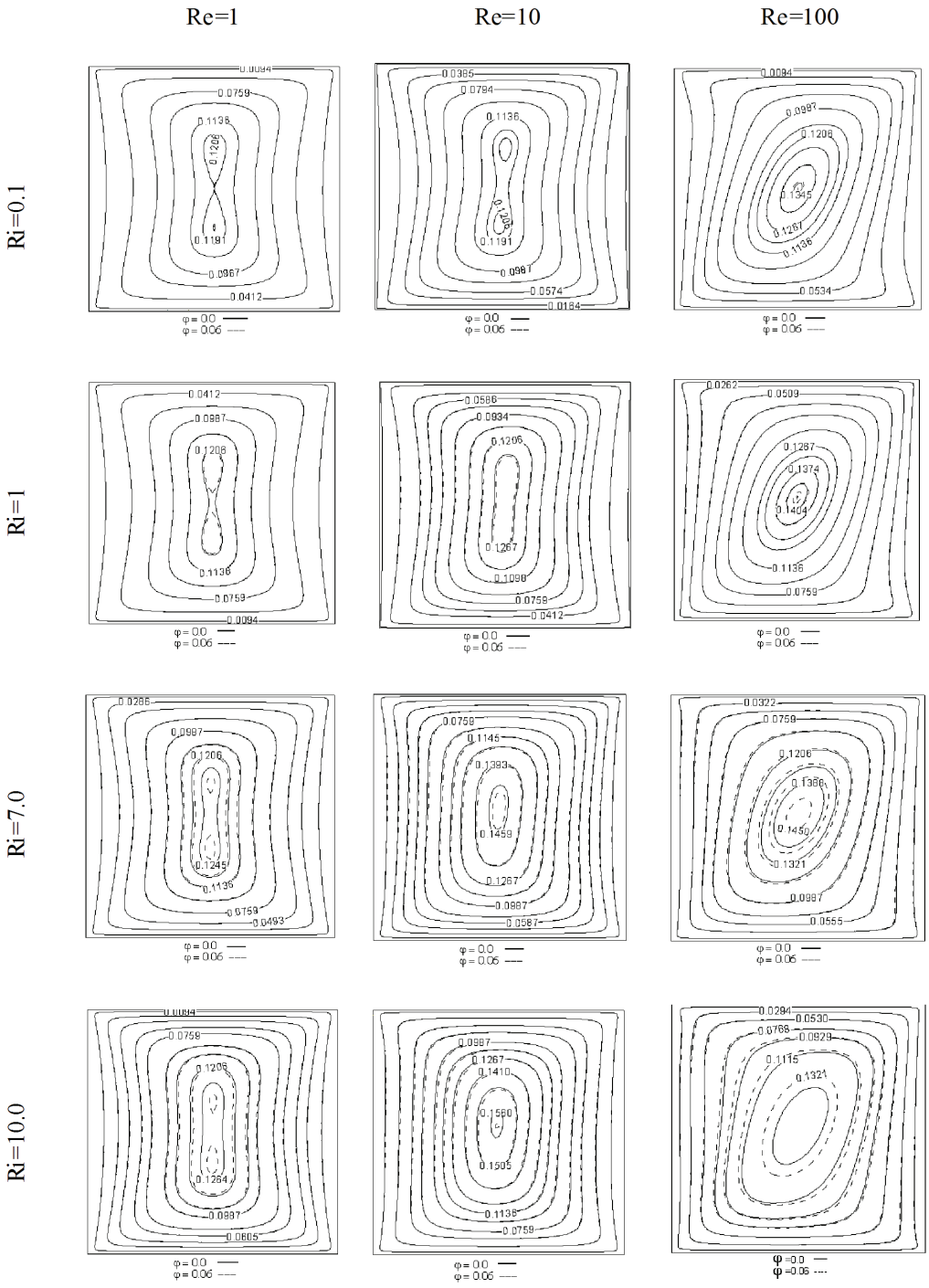

FIG. 4: Streamlines at $\gamma = 30^{o}$ and different values of Ri and Re numbers

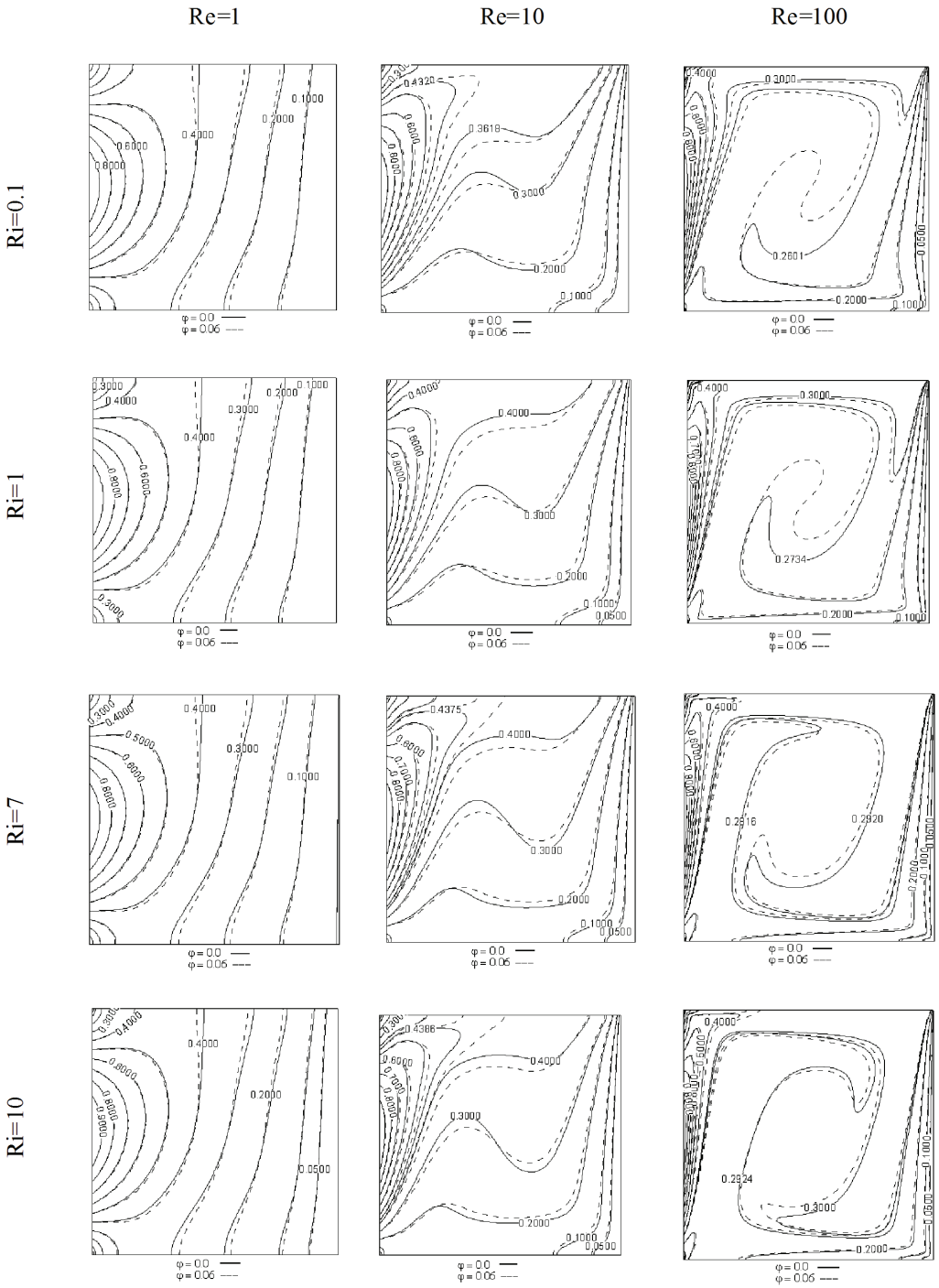

FIG. 5: Isotherms at $\gamma = 30^{o}$ and different values of Ri and Re numbers

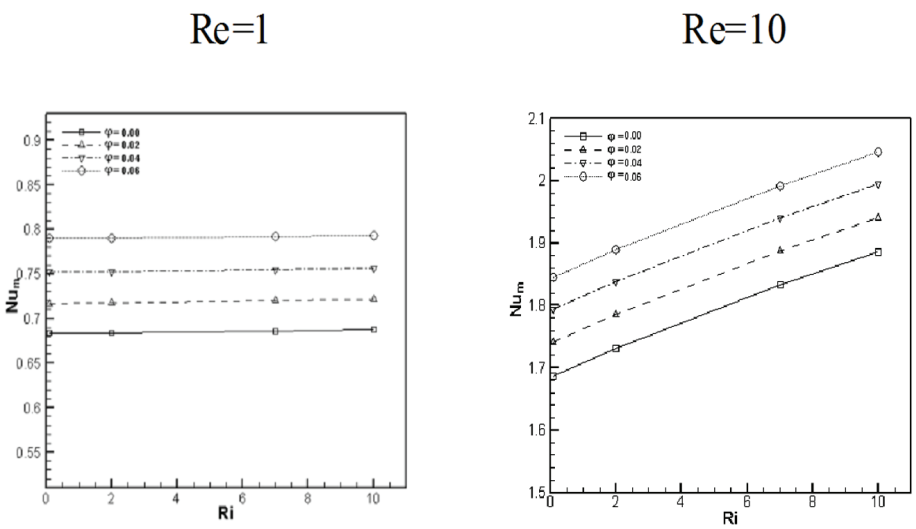

FIG. 6: Variations of average Nusselt number with the volume fraction of nanoparticles at different Ri and Re numbers and $\gamma = 0^o$

For all values of Ri and γ, on increase in Re, the average Nusselt number also increases. Tables 5 to 7 show the variations of the average Nusselt number in percentage.

According to Table 5, for low Re and Ri numbers and on increase in γ from 30^o to 60^o, the average Nusselt number does not change. Note that at low values of the Reynolds and Richardson numbers, forced and natural heat convection are weak and the dominant form of heat transfer is conduction. Thus, variations of the angle do not cause a significant change in the value of the average Nusselt number.

On increase in the Ri number, natural hot convection increases. Since the forced convection tends to make the fluid pass at the heat wall and the natural heat convection tends to make the fluid move upward, the increase in the angle causes the average Nusselt number to increase. At Re = 100, on increase in γ, the average Nusselt number decreases. Except for Ri = 7 and 10, in which case the rate of heat transfer drastically increases according to the temperature and flow fields for this specific case, three vortices are formed inside the cavity instead of a rotational flow.

Therefore, the values of the Nusselt number suddenly increase. Of course, at Ri = 0.1 and 1, the buoyancy force is negligible, and this kind of vertical flow is not formed. In this case, since the buoyancy force is directed somewhat countercurrently to the fluid flow caused by the walls movement, the heat transfer rate decreases on increase in the Ri number from 0.1 to 1. But for the above-mentioned reasons, on further increase in the Richardson number, the average Nusselt number drastically increases. At Re = 10, except at Ri = 0.1 when the average Nusselt number remains unchanged, other values of the average Nusselt number decrease.

TABLE 4: Variation of the average Nusselt numbers at all values of the Ri and Re numbers, φ and γ

		Re = 1.0				Re = 10				Re = 100			
	Φ / Ri	0.0	0.02	0.04	0.06	0.0	0.02	0.04	0.06	0.0	0.02	0.04	0.06
γ = 30°	0.1	0.683	0.717	0.752	0.789	1.687	1.741	1.794	1.845	4.058	4.215	4.371	4.526
	1.0	0.683	0.717	0.753	0.789	1.742	1.796	1.849	1.901	4.434	4.589	4.744	4.896
	7.0	0.686	0.720	0.755	0.792	1.864	1.920	1.974	2.027	5.022	5.186	5.347	5.506
	10.0	0.688	0.721	0.756	0.793	1.927	1.984	2.039	2.092	5.249	5.422	5.591	5.755
γ = 60°	0.1	0.683	0.717	0.752	0.789	1.687	1.741	1.794	1.845	4.051	4.208	4.364	4.519
	1.0	0.683	0.717	0.753	0.789	1.738	1.793	1.846	1.898	4.344	4.501	4.658	4.813
	7.0	0.685	0.719	0.754	0.791	1.852	1.909	1.964	2.018	4.857	5.023	5.186	5.346
	10.0	0.686	0.720	0.755	0.792	1.911	1.968	2.025	2.080	5.083	5.254	5.423	5.588
γ = 90°	0.1	0.683	0.717	0.752	0.789	1.686	1.740	1.793	1.844	4.039	4.197	4.353	4.509
	1.0	0.683	0.717	0.753	0.789	1.720	1.775	1.822	1.880	4.159	4.319	4.479	4.638
	7.0	0.684	0.718	0.753	0.790	1.797	1.855	1.911	1.965	4.424	4.593	4.761	4.927
	10.0	0.684	0.718	0.753	0.790	1.838	1.897	1.954	2.010	4.556	4.732	4.906	5.075
γ = 120°	0.1	0.683	0.717	0.752	0.789	1.685	1.739	1.791	1.843	4.025	4.183	4.339	4.496
	1.0	0.683	0.717	0.752	0.789	1.692	1.746	1.799	1.852	3.880	4.047	4.213	4.378
	7.0	0.682	0.716	0.751	0.789	1.707	1.764	1.820	1.874	5.608	5.769	5.926	6.077
	10.0	0.682	0.716	0.751	0.788	1.715	1.774	1.831	1.886	5.908	6.106	6.215	6.383
γ = 150°	0.1	0.683	0.717	0.752	0.789	1.683	1.737	1.790	1.841	4.013	4.171	4.328	4.484
	1.0	0.683	0.717	0.751	0.789	1.659	1.714	1.767	1.819	3.548	3.717	3.891	4.066
	7.0	0.680	0.715	0.750	0.788	1.588	1.644	1.699	1.752	5.454	5.611	5.761	5.904
	10.0	0.679	0.714	0.749	0.787	1.536	1.593	1.649	1.703	5.869	5.902	6.071	6.232

Variations of the average Nusselt number with φ are presented in Table 6. On increase in φ in each step, the values of the average Nusselt number also increase. In most cases, an increase in the average Nusselt number between a pure fluid and a nanofluid with $\varphi = 0.02$ is greater than the increase in the heat transfer rate between the cases where $\varphi = 0.04$ and $\varphi = 0.06$, while in both cases φ is increased by the same amount.

TABLE 5: Variation of the average Nusselt numbers at all the values of the Ri and Re numbers, φ and γ

		Re = 1.0				Re = 10				Re = 100			
	φ	0	0.02	0.04	0.06	0	0.02	0.04	0.06	0	0.02	0.04	0.06
φ	Ri												
30–60	0.1	0.00	0.00	0.00	0.00	0.00	0.00	0.00	0.00	–0.17	–0.17	–0.16	–0.15
	1	0.00	0.00	0.00	0.00	–0.23	–0.17	–0.16	–0.16	–2.03	–1.92	–1.81	–1.70
	7	–0.15	–0.14	–0.13	–0.13	–0.64	–0.57	–0.51	–0.44	–3.29	–3.14	–3.01	–2.91
	10	–0.29	–0.14	–0.13	–0.13	–0.83	–0.81	–0.69	–0.57	–3.16	–3.10	–3.00	–2.90
60–90	0.1	0.00	0.00	0.00	0.00	–0.06	–0.06	–0.06	–0.05	–0.30	–0.26	–0.25	–0.22
	1	0.00	0.00	0.00	0.00	–1.04	–1.00	–1.30	–0.95	–4.26	–4.04	–3.84	–3.64
	7	–0.15	–0.14	–0.13	–0.13	–2.97	–2.83	–2.70	–2.63	–8.91	–8.56	–8.20	–7.84
	10	–0.29	–0.28	–0.26	–0.25	–3.82	–3.61	–3.51	–3.37	–10.37	–9.94	–9.53	–9.18
90–120	0.1	0.00	0.00	0.00	0.00	–0.06	–0.06	–0.11	–0.05	–0.35	–0.33	–0.32	–0.29
	1	0.00	0.00	–0.13	0.00	–1.63	–1.63	–1.26	–1.49	–6.71	–6.30	–5.94	–5.61
	7	–0.29	–0.28	–0.27	–0.13	–5.01	–4.91	–4.76	–4.63	26.76	25.60	24.47	23.34
	10	–0.29	–0.28	–0.27	–0.25	–6.69	–6.48	–6.29	–6.17	29.68	29.04	26.68	25.77
120–150	0.1	0.00	0.00	0.00	0.00	–0.12	–0.12	–0.06	–0.11	–0.30	–0.29	–0.25	–0.27
	1	0.00	0.00	–0.13	0.00	–1.95	–1.83	–1.78	–1.78	–8.56	–8.15	–7.64	–7.13
	7	–0.29	–0.14	–0.13	–0.13	–6.97	–6.80	–6.65	–6.51	–2.75	–2.74	–2.78	–2.85
	10	–0.44	–0.28	–0.27	–0.13	–10.44	–10.20	–9.94	–9.70	–0.66	–3.34	–2.32	–2.37

TABLE 6: Variations of the average Nusselt number with φ

		Re=1.0			Re=10			Re=100		
γ	φ Ri	0-0.02	0.02-0.04	0.04-0.06	0-0.02	0.02-0.04	0.04-0.06	0-0.02	0.02-0.04	0.04-0.06
30	0.1	4.978	4.881	4.92	3.201	3.044	2.843	3.8689	3.7011	3.546
	1	4.978	5.021	4.781	3.1	2.951	2.812	3.49571	3.3776	3.204
	7	4.956	4.861	4.901	3.004	2.813	2.685	3.26563	3.1045	2.974
	10	4.797	4.854	4.894	2.958	2.772	2.599	3.29587	3.1169	2.933
60	0.1	4.978	4.881	4.92	3.201	3.044	2.843	3.87559	3.7072	3.552
	1	4.978	5.021	4.781	3.165	2.956	2.817	3.61418	3.4881	3.328
	7	4.964	4.868	4.907	3.078	2.881	2.749	3.41775	3.2451	3.085
	10	4.956	4.861	4.901	2.983	2.896	2.716	3.36416	3.2166	3.043
90	0.1	4.978	4.881	4.92	3.203	3.046	2.844	3.91186	3.7169	3.584
	1	4.978	5.021	4.781	3.198	2.648	3.183	3.84708	3.7046	3.55
	7	4.971	4.875	4.914	3.228	3.019	2.826	3.82007	3.6577	3.487
	10	4.971	4.875	4.914	3.21	3.005	2.866	3.86304	3.6771	3.445
120	0.1	4.978	4.881	4.92	3.205	2.99	2.903	3.92547	3.7294	3.618
	1	4.978	4.881	4.92	3.191	3.036	2.946	4.30412	4.1018	3.916
	7	4.985	4.888	5.06	3.339	3.175	2.967	2.8709	2.7214	2.548
	10	4.985	4.888	4.927	3.44	3.213	3.004	3.35139	1.7851	2.703
150	0.1	4.978	4.881	4.92	3.209	3.051	2.849	3.9372	3.7641	3.604
	1	4.978	4.742	4.89	3.315	3.092	2.943	4.76325	4.6812	4.498
	7	5.147	4.895	5.067	3.526	3.345	3.119	2.87862	2.6733	2.482
	10	5.155	4.902	5.073	3.711	3.515	3.275	2.9123	2.8634	2.652

TABLE 7: Variations of the average Nusselt number with Ri

		Re = 1.0				Re = 10				Re = 100			
	φ	0	0.02	0.04	0.06	0	0.02	0.04	0.06	0	0.02	0.04	0.06
γ	Ri												
30	0.1–1	0.00	0.00	0.13	0.00	3.26	3.16	3.07	3.04	9.27	8.87	8.53	8.17
	1–7	0.44	0.42	0.27	0.38	7.00	6.90	6.76	6.63	13.26	13.01	12.71	12.46
	7–10	0.29	0.14	0.13	0.13	3.38	3.33	3.29	3.21	4.52	4.55	4.56	4.52
60	0.1–1	0.00	0.00	0.13	0.00	3.02	2.99	2.90	2.87	7.23	6.96	6.74	6.51
	1–7	0.29	0.28	0.13	0.25	6.56	6.47	6.39	6.32	11.81	11.60	11.34	11.07
	7–10	0.15	0.14	0.13	0.13	3.19	3.09	3.11	3.07	4.65	4.60	4.57	4.53
90	0.1–1	0.00	0.00	0.13	0.00	2.02	2.01	1.62	1.95	2.97	2.91	2.89	2.86
	1–7	0.15	0.14	0.00	0.13	4.48	4.51	4.88	4.52	6.37	6.34	6.30	6.23
	7–10	0.00	0.00	0.00	0.00	2.28	2.26	2.25	2.29	2.98	3.03	3.05	3.00
120	0.1–1	0.00	0.00	0.00	0.00	0.42	0.40	0.45	0.49	–3.60	–3.25	–2.90	–2.62
	1–7	–0.15	–0.14	–0.13	0.00	0.89	1.03	1.17	1.19	44.54	42.55	40.66	38.81
	7–10	0.00	0.00	0.00	–0.13	0.47	0.57	0.60	0.64	5.35	5.84	4.88	5.04
150	0.1–1	0.00	0.00	–0.13	0.00	–1.43	–1.32	–1.28	–1.20	–11.59	–10.88	–10.10	–9.32
	1–7	–0.44	–0.28	–0.13	–0.13	–4.28	–4.08	–3.85	–3.68	53.72	50.96	48.06	45.2
	7–10	–0.15	–0.14	–0.13	–0.13	–3.27	–3.10	–2.94	–2.80	7.61	5.19	5.38	5.56

Variations of the average Nusselt number with Ri are listed in Table 7. Except for those cases which are presented in bold, on increase in the Ri number, the heat transfer rate increases. It can be understood that most of the decreased values are obtained-ed at $\gamma = 150^{o}$ and $\gamma > 90^{o}$ at all the values of Re and heat transfer rate increases with Ri.

5. CONCLUSIONS

The problem of mixed convection of a SiO_2–water nanofluid in an inclined double lid-driven square cavity with sinusoidal heating on the left wall was investigated numerically using the finite volume method. The effects of the Richardson number, Reynolds number, and volume fraction of nanoparticles on the fluid flow and heat transfer characteristics were studied and the following results were obtained: Both the Richardson and Reynolds numbers, as well as the volume fraction of nanoparticles and the cavity inclination angles influence the streamline pattern, temperature field, and heat transfer rate inside the cavity. At low Re and Ri numbers, on increase in γ, the average Nusselt number does not change with increase in the cavity inclination angles.

At low Reynolds numbers, the heat transfer rate does not change noticeably with increase in Richardson number, while with increase in the Richardson number at high Reynolds numbers it is enhanced. For all the Reynolds and Richardson numbers considered, the rate of heat transfer increases with the volume fraction of SiO_2 nanoparticles.

REFERENCES

Aydin, O., Aiding and opposing mechanisms of mixed convection in a shear and buoyancy-driven cavity, *Int. Commun. Heat Mass Transfer*, vol. 26, no. 7, pp. 1019–1028, 1999.

Basak, T., Roy, S., and Balakrishnan, A. R., Effects of thermal boundary conditions on natural convection flows within a square cavity, *Int. J. Heat Mass Transfer*, vol. 49, pp. 4525–4535, 2006.

Basak, T., Roy, S., Sharma, P. K., and Pop, I., Analysis of mixed convection flows within a square cavity with uniform and nonuniform heating of bottom wall, *Int. J. Thermal Sci*., vol. 48, pp. 891–912, 2009.

Cha, C. K. and Jaluria, Y., Recirculating mixed convection flow for energy extraction, *Int. J. Heat Mass Transfer*, vol. 27, pp. 1801–1810, 1984.

Choi, S. U. S., Enhancing thermal conductivity of fluids with nanoparticles, in: D. A. Siginer and H. P. Wang (Eds.), *Developments and Applications of Non-Newtonian Flows*, FED, vol. 231/MD–vol. 66, ASME, New York, pp. 99–105, 1995.

De Vahl Davis, G., Natural convection of air in a square cavity: a benchmark solution, *Int. J. Numer. Meth. Fluids*, vol. 3, pp. 249–264, 1983.

Eastman, J. A., Choi, S. U. S., Li, S., Yu, W., and Thompson, L. J., Anomalously increased effective thermal conductivities of ethylene glycol-based nanofluids containing copper nanoparticles, *Appl. Phys. Lett*., vol. 78, pp. 718–720, 2001.

Fusegi, T., Kuwahara, K., and Farouk, B., A numerical study of three-dimensional natural convection in a differentially heated cubic enclosure, *Int. J. Heat Mass Transfer,* vol. 34, no. 6, pp. 1543–1557, 1991.

Ghasemi, B. and Aminossadati, S. M., Mixed convection in a lid-driven triangular enclosure filled with nanofluids, *Int. Commun. Heat Mass Transfer*, vol. 37 1142–1148, 2010.

Ha, M. Y. and Jung, M. J., A numerical study of three-dimensional conjugate heat transfer of natural convection and conduction in a differentially heated cubic enclosure with a heat-generating cubic conducting body, *Int. J. Heat Mass Transfer*, vol. 43, pp. 4229–4248, 2000.

Hadjisophocleous, G. V., Sousa, A. C. M., and Venart, J. E. S., Predicting the transient natural convection in enclosures of arbitrary geometry using a nonorthogonal numerical model, *Numer. Heat Transfer*, Part A, vol. 13, pp. 373–392, 1998.

Hwang, K. S., Lee, J. H., and Jang, S. P., Buoyancy-driven heat transfer of water-based Al_2O_3 nanofluids in a rectangular cavity, *Int. J. Heat Mass Transfer*, vol. 50, nos. 19–20, pp. 4003–4010, 2007.

Ideriah, F. J. K., Prediction of turbulent cavity flow driven by buoyancy and shear, *J. Mech. Eng. Sci*., vol. 22, pp. 287–295, 1980.

Imberger, J. and Hamblin, P. F., Dynamics of lakes, reservoirs, and cooling ponds, *Annu. Rev. Fluid Mech*., vol. 14, pp. 153–187, 1982.

Lee, S., Choi, S. U. S., Li, S., and Eastman, J. A., Measuring thermal conductivity of fluids containing oxide nanoparticles, *J. Heat Mass Transfer*, vol. 121, pp. 280–289, 1999.

Mahmoodi, M., Mixed convection inside nanofluid filled rectangular enclosures with moving bottom wall, *Thermal Sci*., vol. 15, pp. 889–903, 2011.

Maiga, S. E. B., Palm, S. J., Nguyen, C. T., Roy, G., and Galanis, N., Heat transfer enhancement by using nanofluids in forced convection flows, *Int. J. Heat Fluid Flow*, vol. 26, pp. 530–546, 2005.

Mansour, M. A., Mohamed, R. A., Abd-Elaziz, M. M., and Ahmed, S. E., Numerical simulation of mixed convection flows in a square lid-driven cavity partially heated from below using nanofluid, *Int. Commun. Heat Mass Transfer*, vol. 37, pp. 1504–1512, 2010.

Markatos, N. C. and Pericleous, K. A., Laminar and turbulent natural convection in an enclosed cavity, *Int. J. Heat Mass Transfer*, vol. 27, no. 5, pp. 755–772, 1984.

Masuda, H., Ebata, A., Teramae, K., and Hishinuma, N., Alteration of thermal conductivity and viscosity of liquid by dispersing ultra-fine particles, *Netsu Bussei*, vol. 7, no. 4, pp. 227–233, 1993.

Moallemi, M. K. and Jang, K. S., Prandtl number effects on laminar mixed convection heat transfer in a lid-driven cavity, *Int. J. Heat Mass Transfer*, vol. 35, pp. 1881–1892, 1992.

Mohamad, A. A. and Viskanta, R., Flow and heat transfer in a lid-driven cavity filled with a stably stratified fluid, *Appl. Math. Model*., vol. 19, pp. 465-472, 1995.

Muthtamilselvan, M., Kandaswamy, P., and Lee, J., Heat transfer enhancement of copper–water nanofluids in a lid–driven enclosure, *Commun Nonlinear Sci. Numer. Simul*., vol. 15, pp. 1501–1510, 2010.

Oztop, H. F., Abu-Nada, E., Varol, Y., and Al-Salem, Kh., Computational analysis of nonisothermal temperature distribution on natural convection in nanofluid filled enclosures, *Superlattices Microstructures*, vol. 49, pp. 453–467, 2011.

Pilkington, L. A. B., Review lecture: The float glass process, *Proc. Roy. Soc. London A*, vol. 314, pp. 1–25, 1969.

Rahman, M. D. M., Alim, M. A., Saha, S., and Chowdhury, M. K., A numerical study of mixed convection in a square cavity with a heat conducting square cylinder at different locations, *J. Mech. Eng*., vol. ME39, no. 2, pp. 78–85, 2008.

Sarris, I. E., Lekakis I., and Vlachos, N. S., Natural convection in a 2D enclosure with sinusoidal upper wall temperature, *Numer. Heat Transfer*, Part A, vol. 42, pp. 513–530, 2002.

Sathiyamoorthy, M., Basak, T., Roy, S., and Pop, I., Steady natural convection flows in a square cavity with linearly heated side wall(s), *Int. J. Heat Mass Transfer*, vol. 50, pp. 766–775, 2007.

Sebdani, M. S., Mahmoodi, M., and Hashemi, S. M., Effect of nanofluid variable properties on mixed convection in a square cavity, *Int. J. Thermal Sci*., vol. 52, pp. 112–126, 2012.

Sharif, M. A. R., Laminar mixed convection in shallow inclined driven cavities with hot moving lid on top and cooled from bottom, *Appl. Thermal Eng*., vol. 27, pp. 1036–1042, 2007.

Sivasankaran, S., Malleswaran, A., Lee, J., and Sundar, P., Hydro-magnetic combined convection in a lid-driven cavity with sinusoidal boundary conditions on both sidewalls, *Int. J. Heat Mass Transfer*, vol. 54, pp. 512–525, 2011.

Tiwari, R. K. and Das, M. K., Heat transfer augmentation in a two-sided lid–driven differentially heated square cavity utilizing nanofluids, *Int. J. Heat Mass Transfer*, vol. 50, pp. 2002–2018, 2007.

Wen, D. and Ding, Y., Formulation of nanofluids for natural convective heat transfer applications, *Int. J. Heat Fluid Flow*, vol. 26, no. 6, pp. 855–864, 2005.

Xuan, Y. M. and Li, Q., Heat transfer enhancement of nanofluids, *Int. J. Heat Fluid Flow*, vol. 21, pp. 58–64, 2000.

Zarei, A. H., Rostamian, S. H., and Esfe, H. M., Heat transfer behavior of mixed convection flow in lid-driven cavity containing hot obstacle subjected to nanofluid with variable properties, *J. Basic Appl. Sci. Res.*, vol. 3, no. 2, pp. 713–721, 2013.